PTEP

Prog. Theor. Exp. Phys. **2024** 123A02 (23 pages)
DOI: 10.1093/ptep/ptae157

Thermophysical Properties and Mass Spectra of Meson Systems via the Nikiforov–Uvarov Method

Ridha Horchani[1,⋆], Omama Al Kharusi[1], Akpan N. Ikot[2,3], and Faizuddin Ahmed[4]

[1] *Department of Physics, College of Science, Sultan Qaboos University, PO Box 36, Al-Khod 123, Muscat, Sultanate of Oman*
[2] *Theoretical Physics Group, Department of Physics, University of Port Harcourt, Choba 500102, Nigeria*
[3] *Western Caspian University, Baku AZ1000, Azerbaijan*
[4] *Department of Physics, University of Science and Technology Meghalaya, Ri-Bhoi 793101, India*
⋆Email: horchani@squ.edu.om

Received July 28, 2024; Revised October 14, 2024; Accepted October 21, 2024; Published October 23, 2024

In this study, we analyze the mass spectra of meson systems within an N-dimensional space using the Killingbeck potential combined with an inversely quadratic potential. We employ the Nikiforov–Uvarov method along with the Pekeris approximation scheme to account for the centrifugal barrier. This approach enables us to compute numerical energy eigenvalues, normalized eigenfunctions, and mass spectra for both heavy and heavy–light meson systems. We explore various scenarios of the potential and find that the resulting energy eigenvalues are consistent with those obtained through previous analytical methods and experimental data. Additionally, we compute the thermodynamic properties of quarkonium particles, including mean energy, specific heat, free energy, and entropy. Furthermore, we investigate the effects of temperature and the dimensional number on meson masses and thermodynamic properties, providing valuable insights into the behavior of meson systems under different conditions.

Subject Index A73, A13

1. Introduction

Over the course of several decades, researchers have increasingly delved into exploring the analytical solutions of the Schrödinger equation for various physical potential models within quantum mechanical systems. Researchers in multiple branches of physics, including nuclear physics, atomic physics, and quantum chromodynamics (QCD), have shown keen interest in nonrelativistic wave equations and energy eigenvalues. Quantum chromodynamics (QCD) theory serves as a valuable framework for understanding the strong force, with hadron spectroscopy playing a pivotal role in both the nonperturbative and perturbative regimes. Recent advancements in experimental techniques at Belle, BES, CLEO, CDF, LHC, and BaBar have yielded enormous amounts of data, revealing many unexpected findings [1–5]. Several new states, particularly within the meson sector, have been observed that do not fit into the conventional $q\bar{q}$ scheme. All these exotic states, which do not fit into the qqq and $q\bar{q}$ schemes, require further theoretical investigation [6–13]. Numerous aspects of these systems can be investigated by using the nonrelativistic Schrödinger equation, assuming that the quark–antiquark strong interaction is described by a phenomenological potential. Several potential models offer robust descriptions of meson mass spectra. However, it is essential for these potential models to embody

asymptotic freedom and confinement as essential features of strong interactions. When simulating the interaction potentials for these systems, confinement-type potentials are typically employed. The potential forms can vary, e.g. Martin, logarithmic, and Cornell potentials [14–18]. For such systems, a successful potential model is one that agrees with the experimental results within about 20 MeV [19]. The principal challenge in such studies arises from the absence of exact solutions to the Schrödinger equation for these systems, particularly when the centrifugal potential is included. To overcome this problem, researchers often resort to solving the wave equation approximately using various techniques, both analytical and numerical [20]. These include the Nikiforov–Uvarov (NU) method [20–25], the asymptotic iterative method (AIM) [26], the analytical exact iterative method (AEIM) [27], the Wentzel–Kramers–Brillouin method (WKB) [28], the Laplace transformation method (LTM) [29], and the artificial neural network method (ANN) [30].

It is noteworthy that meson masses have been widely investigated at finite temperature within the framework of the linear sigma model in numerous works, e.g. Refs. [31–33].

In this study, we have investigated the mass spectra of meson systems by solving the N-dimensional Schrödinger equation under the interaction of the Killingbeck potential plus an inversely quadratic potential (KPIQP) within the framework of the Nikiforov–Uvarov method, and by using the Pekeris approximation scheme to account for the centrifugal barrier.

Additionally, we have examined the influence of the dimensional number on meson mass. As a natural consequence of the unification of the two modern theories of quantum mechanics and relativity, and the emergence of string theory, the investigation of Standard Model particles in extra- or higher-dimensional space has become a hot topic. Recent works [34, 35] have focused on the investigation of quarkonium in higher-dimensional space and have shown that the dimensional number plays a crucial role in altering binding energy and dissociation temperatures. From an experimental point of view, the investigation of the existence of extra dimensions is one of the primary goals of the LHC. The search for extra dimensions with the ATLAS and CMS detectors is discussed in Ref. [36].

The obtained energies were then used to study the thermodynamic properties of mesons. This is motivated by the significant role that thermodynamic properties play in describing the quark–gluon plasma. For example, Modarres and Mohamadnejad [37] studied the thermodynamic properties of the quark–gluon plasma, as well as its phase diagram as a function of baryon density and temperature. Furthermore, thermodynamic properties are investigated within the framework of chiral quark models and in molecular physics using both relativistic and nonrelativistic models [38, 39].

The KPIQP has the form [23, 27] of

$$V_{\mathrm{KPIQP}}(r) = V_{\mathrm{KP}}(r) + V_{\mathrm{IQP}}(r) = A\,r^2 + B\,r - \frac{C}{r} + \frac{D}{r^2}, \tag{1}$$

where $V_{\mathrm{KP}}(r) = (A\,r^2 + B\,r - \frac{C}{r})$ is the Killingbeck potential and $V_{\mathrm{IQP}}(r) = \frac{D}{r^2}$ is the inversely quadratic potential. Here A, B, C, and D are positive potential parameters that will be determined based on experimental data at a later stage.

When $A = B = D = 0$, the KPIQP reduces to the Coulomb potential commonly employed in describing the hydrogenic atom. When $A = D = 0$, the KPIQP simplifies to the Cornell po-

tential, where C represents a coupling constant and B denotes a linear confinement parameter. It is noteworthy that the Cornell potential is the sum of two components: a coulombic term $(-\frac{C}{r})$, resulting from one-gluon exchange between quarks and antiquarks at short distances [40], and a linear term $(B\,r)$, which represents quark confinement at larger distances [41].

To improve the behavior of the potential in the region as $r \to 0$ and provide better confinement, two terms are added to the Cornell potential: the inversely quadratic potential (the term D/r^2) and the harmonic oscillator term. The KPIQP has also been used to compute the energy eigenvalue spectra of quantum dot systems [42, 43] and diatomic molecules [44]. Recently, Khokha et al. analytically determined meson mass spectra by solving the N-dimensional radial Schrödinger equation with the KPIQP using the exact iteration method [27].

The paper is structured as follows: In Section 2, we derive the bound state solutions of the Schrödinger equation with the KPIQP using the Nikiforov–Uvarov (NU) method in N-dimensional space. We discuss special cases of the obtained energy eigenvalues. In Section 3, we present numerical results for the masses of the charmonium ($c\bar{c}$), bottomonium ($b\bar{b}$), bottom–charm ($b\bar{c}$), and charm–strange ($c\bar{s}$) mesons. These results are compared with those obtained from other analytical methods and available experimental data. The derivation and discussion of the expressions for the thermodynamic properties of quarkonium particles are also discussed in section 3. Finally, Section 4 provides a summary and conclusion of the paper.

2. Theory

2.1 *Bound state solutions of the Schrödinger equation*

In this study, we employ the Nikiforov–Uvarov (NU) method to solve a second-order differential equation of the hypergeometric type. A comprehensive description of the methodology can be found in the appendix. In N-dimensional Hilbert space, the Schrödinger equation describing the interaction between two particles via a spherically symmetric potential can be written as in Ref. [45]:

$$\psi^{''(r)} + \left(\frac{N-1}{r}\right)\psi'(r) + \left(\frac{2\mu}{\hbar^2}(E_{n\ell} - V(r)) - \frac{\ell(\ell+N-2)}{r^2}\right)\psi(r) = 0 \tag{2}$$

where $\mu = m_q m_{\bar{q}}/(m_q + m_{\bar{q}})$ is the reduced mass of the system, ℓ is the angular momentum quantum number, and $E_{n\ell}$ is the energy eigenvalue with the corresponding radial wave function $\psi(r)$.

Setting the wave function $\psi(r) = r^{\frac{1-N}{2}}R(r)$, the following radial Schrödinger equation is obtained:

$$R''(r) + \left(\frac{2\mu}{\hbar^2}(E_{n\ell} - V(r)) - \frac{(N+2\ell-1)(N+2\ell-3)}{4r^2}\right)R(r) = 0. \tag{3}$$

Substituting Eq. (1) into Eq. (3), we obtain

$$R''(r) + \left(\frac{2\mu E_{n\ell}}{\hbar^2} + \frac{2\mu A}{\hbar^2}r^2 - \frac{2\mu B}{\hbar^2}r + \frac{2\mu C}{\hbar^2}\frac{1}{r} - \left(\frac{2\mu D}{\hbar^2} + \frac{(N+2\ell-1)(N+2\ell-3)}{4}\right)\frac{1}{r^2}\right)R(r) = 0. \tag{4}$$

Equation (4) can be simplified to the following equation:

$$R''(r) + \left(\varepsilon_{n\ell} + ar^2 - br + \frac{c}{r} - \frac{d}{r^2}\right)R(r) = 0 \tag{5}$$

where $\varepsilon_{n\ell} = \frac{2\mu E_{n\ell}}{\hbar^2}$, $a = \frac{2\mu A}{\hbar^2}$, $b = \frac{2\mu B}{\hbar^2}$, $c = \frac{2\mu C}{\hbar^2}$, $d = \frac{2\mu D}{\hbar^2} + \frac{(N+2\ell-1)(N+2\ell-3)}{4}$.

Using the change of variable $x = \frac{1}{r}$, Eq. (4) reduces to

$$R''(x) + \frac{2x}{x^2}R'(x) + \frac{1}{x^4}\left(\varepsilon_{n\ell} + cx - \frac{b}{x} + \frac{a}{x^2} - dx^2\right)R(x) = 0. \tag{6}$$

Equation (6) can be solved using the conventional Nikiforov–Uvarov approach for solving second-order differential equations of hypergeometric type. However, we must put the equation into a standard form using an approximation scheme by expanding $\frac{b}{x}$ and $\frac{a}{x^2}$ in power series to second-order around r_0 ($\delta = \frac{1}{r_0}$ where r_0 is the characteristic radius of the meson). Thus we can write

$$\frac{b}{x} = b\left(\frac{3}{\delta} - \frac{3x}{\delta^2} + \frac{x^2}{\delta^3}\right) \tag{7 a}$$

$$\frac{a}{x} = a\left(\frac{6}{\delta^2} - \frac{8x}{\delta^3} + \frac{3x^2}{\delta^4}\right). \tag{7 b}$$

This approximation is suitable for obtaining local solutions of the Schrödinger equation, when the range of the distance r is not far from its equilibrium position. We note that the validity of this approximation depends on the magnitude of the rotational quantum number ℓ. In fact the relative discrepancies are multiplied by the factor $\ell(\ell+1)$. In the present work, we are studying the upper limit of the quantum number ℓ so we can safely use this approximation.

Inserting Eqs. (7 a) and (7 b) into Eq. (6) results in

$$R''(x) + \frac{2x}{x^2}R'(x) + \frac{1}{x^4}\left(-\varepsilon + Q\,x - P\,x^2\right)R(x) = 0, \tag{8}$$

where

$$\varepsilon = -\varepsilon_{n\ell} + \frac{3b}{\delta} - \frac{6a}{\delta^2} \tag{9}$$

$$Q = \frac{3b}{\delta^2} - \frac{8a}{\delta^3} + a \tag{10}$$

$$P = \frac{b}{\delta^3} - \frac{3a}{\delta^4} + d. \tag{11}$$

Equation (8) is a standard form of the hypergeometric differential equation; it has the same shape as Eq. (A2) with the following parameters:

$$\tilde{\sigma}(x) = \left(-\varepsilon + Qx - Px^2\right) \tag{12}$$

$$\sigma(x) = x^2 \tag{13}$$

$$\tilde{\tau}(x) = 2x. \tag{14}$$

Substituting Eqs. (12), (13), and (14) into Eq. (A10), we obtain the polynomial $\pi(x)$ as

$$\pi(x) = \pm\sqrt{(k+P)x^2 - Qx + \varepsilon}. \tag{15}$$

Since $\pi(x)$ is a first-order polynomial, the terms under the square root must be equated to the square of a linear function in x, say $(Zx + q)^2$. Using this condition $(Zx + q)^2 = (k+P)x^2 - Qx + \varepsilon$ and solving completely, we find

$$k = \frac{Q^2}{4\varepsilon} - P. \tag{16}$$

Substituting Eq. (16) into Eq. (15) with simplifications yields $\pi(x)$:

$$\pi(x) = \pm\frac{Q}{2\sqrt{\varepsilon}}\left(x - \frac{2\varepsilon}{Q}\right). \tag{17}$$

In Eq. (17), we choose the value of $\pi(x) = -\frac{Q}{2\sqrt{\varepsilon}}(x - \frac{2\varepsilon}{Q})$ that will give $\frac{d\tau(x)}{dx} < 0$. Then $\tau(x)$ can be written, according to Eq. (A8), as

$$\tau(x) = 2x - \frac{2Q}{\sqrt{\varepsilon}}\left(x - \frac{2\varepsilon}{Q}\right). \tag{18}$$

Upon differentiation of Eq. (18) with respect to x, we obtain:

$$\tau'(x) = 2 - \frac{2Q}{\sqrt{\varepsilon}}. \tag{19}$$

Referring to Eq. (A11), we define the constant λ as

$$\lambda = \frac{Q^2}{2\varepsilon} - P - \frac{2Q}{\sqrt{\varepsilon}}. \tag{20}$$

Upon differentiation of $\sigma(x)$ with respect to x from Eq. (13), we obtain

$$\sigma''(x) = 2. \tag{21}$$

Substituting Eqs. (19) and (21) into Eq. (A12), we obtain

$$\lambda_n = -n\left(2 - \frac{2Q}{\sqrt{\varepsilon}}\right) - n(n-1). \tag{22}$$

By equating Eqs. (20) and (22), we find

$$\sqrt{\varepsilon} = \frac{Q}{2\left(n + \frac{1}{2} \pm \sqrt{P + \frac{1}{4}}\right)}. \tag{23}$$

Inserting the constants P, Q, and ε given in Eqs. (9)–(11), Eq. (23) yields

$$\varepsilon_{n\ell} = \frac{3b}{\delta} - \frac{6a}{\delta^2} - \left(\frac{c + \frac{3b}{\delta^2} - \frac{8a}{\delta^3}}{2n + 1 + \sqrt{\frac{4b}{\delta^3} - \frac{12a}{\delta^4} + 4d + 1}}\right)^2. \tag{24}$$

Using the parameters for a, b, c, and d in Eq. (5) in Eq. (24) with some simplifications, the energy spectra of the meson system are obtained in the N-dimensional space in terms of the KPIQP constants as

$$E_{n\ell} = \frac{3B}{\delta} - \frac{6A}{\delta^2} - \frac{2\mu}{\hbar^2}\left[\frac{\left(\frac{3B}{\delta^2} - \frac{8A}{\delta^3} + C\right)}{(2n+1) + \sqrt{\frac{8\mu B}{\hbar^2\delta^3} - \frac{24\mu A}{\hbar^2\delta^4} + \frac{8\mu D}{\hbar^2} + ((N + 2\ell - 1)(N + 2\ell - 3) + 1)}}\right]^2. \tag{25}$$

When we set $N = 3$ in Eq. (25), we obtain the results in Ref. [46].

To find the radial eigenfunctions, the relevant $\pi(x)$ function must satisfy the following condition (see Eq. (A5)):

$$\frac{\phi_n'(x)}{\phi_n(x)} = \frac{\pi(x)}{\sigma(x)} = \frac{-\left(\frac{Qx}{2\sqrt{\varepsilon}} - \sqrt{\varepsilon}\right)}{x^2} = -\left(\frac{Q}{2x\sqrt{\varepsilon}} - \frac{\sqrt{\varepsilon}}{x^2}\right). \tag{26}$$

Solving a first-order differential equation, we obtain:

$$\phi_n(x) = x^{\frac{-Q}{2\sqrt{\varepsilon}}} e^{-\frac{\sqrt{\varepsilon}}{x}}. \tag{27}$$

The other part of the wave function $y_n(x)$ is the hypergeometric type given by Eq. (A13):

$$y_n(x) = \frac{B_n}{\rho(x)}\frac{d^n}{dx^n}(\sigma^n(x)\rho(x)). \tag{28}$$

Here, B_n represents a normalizing constant, and $\rho(x)$ denotes the weight function, which is the solution of the Pearson differential equation. The Pearson differential equation and $\rho(x)$ for our problem is given by Eq. (A14): $(\sigma\rho)' = \tau\ \rho$. Hence, we use Eq. (A14) to find the second part of the wave function based on the definition of the weight function:

$$\rho\,(x) = x^{-\frac{Q}{\sqrt{\varepsilon}}} e^{-2\frac{\sqrt{\varepsilon}}{x}}. \tag{29}$$

Taking into account both components of the wave function $\phi_n(x)$ and $y_n(x)$ within Eq. (A3), we derive the following expression:

$$\psi_n\,(x) = B_n x^{\frac{Q}{2\sqrt{\varepsilon}}} e^{\frac{\sqrt{\varepsilon}}{x}} \frac{d^n}{dx^n}\left(x^{2n-\frac{Q}{\sqrt{\varepsilon}}} e^{-2\frac{\sqrt{\varepsilon}}{x}}\right). \tag{30}$$

As the last step, we do the replacement $x = 1/r$, and using $\psi_n(r) = rR_n(r)$ in Eq. (30) we get the following:

$$\psi_n\,(x) = B_n r^{-\frac{Q}{2\sqrt{\varepsilon}}} e^{r\sqrt{\varepsilon}}\left(-r^2\frac{d}{dr}\right)^n\left(r^{-2n+\frac{Q}{\sqrt{\varepsilon}}} e^{-2r\sqrt{\varepsilon}}\right). \tag{31}$$

The final form of the radial wave function $\psi_n(r)$ can be written as:

$$\psi_n\,(x) = B_n r^{-1-\frac{Q}{2\sqrt{\varepsilon}}} e^{r\sqrt{\varepsilon}}\left(-r^2\frac{d}{dr}\right)^n\left(r^{-2n+\frac{Q}{\sqrt{\varepsilon}}} e^{-2r\sqrt{\varepsilon}}\right) \tag{32}$$

where B_n is a normalization constant that can be obtained using the condition for the probability of finding a quantum particle in space:

$$\int_0^\infty |\psi_n\,(r)|^2 dr = 1. \tag{33}$$

Special cases:

- *S-wave:* If we set $N = 3$ and $\ell\ =\ 0$ in Eq. (25), we obtain the energy eigenvalue equation for the s-wave of the KPIQP as

$$E_{n0} = \frac{3B}{\delta} - \frac{6A}{\delta^2} - \frac{2\mu}{\hbar^2}\left[\frac{\left(\frac{3B}{\delta^2} - \frac{8A}{\delta^3} + C\right)}{(2n+1) + \sqrt{\frac{8\mu B}{\hbar^2\delta^3} - \frac{24\mu A}{\hbar^2\delta^4} + \frac{8\mu D}{\hbar^2} + 1}}\right]^2. \tag{34}$$

- *Killingbeck potential*: By taking $D\ =\ 0$ and $N\ =\ 3$ in Eq. (25), we obtain the energy eigenvalues for the Killingbeck potential:

$$E_{n\ell} = \frac{3B}{\delta} - \frac{6A}{\delta^2} - \frac{2\mu}{\hbar^2}\left[\frac{\left(\frac{3B}{\delta^2} - \frac{8A}{\delta^3} + C\right)}{(2n+1) + \sqrt{\frac{8\mu B}{\hbar^2\delta^3} - \frac{24\mu A}{\hbar^2\delta^4} + (4\ell\,(\ell+1)+1)}}\right]^2. \tag{35}$$

- *Cornell potential*: By taking $A = D\ =\ 0$ and $N\ =\ 3$ in Eq. (25), we obtain the energy eigenvalues for the Cornell potential:

$$E_{nl} = \frac{3B}{\delta} - \frac{2\mu}{\hbar^2}\left[\frac{\left(\frac{3B}{\delta^2} + C\right)}{(2n+1) + \sqrt{\frac{8\mu B}{\hbar^2\delta^3} + (4\ell\,(\ell+1)+1)}}\right]^2. \tag{36}$$

- *Kratzer-type potential*: By taking $A = B\ =\ 0$ and $N\ =\ 3$ in Eq. (25), we obtain the energy eigenvalues for the Kratzer-type potential:

$$E_{n\ell} = -\frac{2\mu}{\hbar^2}\left[\frac{C}{(2n+1) + \sqrt{\frac{8\mu D}{\hbar^2} + (4\ell\,(\ell+1)+1)}}\right]^2. \tag{37}$$

- *Coulomb potential*: By taking $A = B = D = 0$, $C = Ze^2$, and $N = 3$ in Eq. (25), we obtain the energy eigenvalues for the Coulomb potential:

$$E_{n\ell} = -\frac{2\mu}{\hbar^2}\left[\frac{Ze^2}{(2n+1)+\sqrt{(4\ell\,(\ell+1)+1)}}\right]^2 - \frac{2\mu}{\hbar^2}\left[\frac{Ze^2}{(2n+1)+\sqrt{4\left(\ell+\frac{1}{2}\right)^2}}\right]^2$$
$$= -\frac{\mu}{\hbar^2}\left[\frac{Ze^2}{n+\ell+1}\right]^2 = -\frac{\mu Z^2 e^4}{\hbar^2 n_p^2} \tag{38}$$

where $n_p = n + \ell + 1$ is the principal quantum number, Z is the atomic number, and e is the charge of the electron.

2.2 *Mass spectra of meson systems*

The mass spectra can be obtained by using the approach from Refs. [47, 48]:

$$M_{n\ell} = m_q + m_{\bar{q}} + E_{n\ell} \tag{39}$$

where m_q, $m_{\bar{q}}$, and E_{nl} are the masses of the quark and antiquark, and the derived energy eigenvalues, respectively.

Inserting Eq. (25) into Eq. (39), we obtain the mass spectrum of the meson systems for any arbitrary radial and angular momentum quantum numbers in N-dimensional space as follows:

$$M_{n\ell} = m_q + m_{\bar{q}} + \frac{3B}{\delta} - \frac{6A}{\delta^2} - \frac{2\mu}{\hbar^2}\left[\frac{\left(\frac{3B}{\delta^2} - \frac{8A}{\delta^3} + C\right)}{(2n+1)+\sqrt{\frac{8\mu B}{\hbar^2\delta^3} - \frac{24\mu A}{\hbar^2\delta^4} + \frac{8\mu D}{\hbar^2} + ((N+2\ell-1)\,(N+2\ell-3)+1)}}\right]^2. \tag{40}$$

2.4 *Mass–radius relationship*

In this section, we examine the mass–radius relationship by using the virial theorem for each given eigenstate $|\psi\rangle$ [49]. It is worth noting that the term "radius" means the average distance between the quark and antiquark (or the root mean square radius). We note that defining the charmonium (bottomonium) root mean square radius $r_{\rm rms}$ (or $\langle r\rangle$) is one of the basic properties of charmonium (bottomonium). If the distance between the quark and antiquark in charmonium (bottomonium) is r, charmonium (bottomonium) may be considered to have the radius $r/2$ fm. The root mean square radii, $r_{\rm rms}$, can be directly obtained from the numerical solution of the radial equation with the normalized Schrödinger wave equation:

$$(r_{\rm rms})^2 = \int_0^\infty r^2 |R_{nl}\,(r)|^2 dr \tag{41}$$

where the symbols n and l stand for the principal and orbital angular momentum quantum numbers of the meson, respectively.

The relation of the mean kinetic energy, KE, and the potential energy is given by:

$$\langle KE\rangle = \langle\psi|KE|\psi\rangle = \frac{1}{2}\left\langle\psi\left|r\frac{dV\,(r)}{dr}\right|\psi\right\rangle, \tag{42}$$

In the case of V_{KPIQP}, we obtain

$$E = \langle\psi|KE|\psi\rangle + \langle\psi|V|\psi\rangle = \frac{1}{2}\left\langle\psi|r\frac{dV(r)}{dr}|\psi\right\rangle + \langle\psi|V|\psi\rangle = 2A\left\langle r^2\right\rangle + \frac{3B}{2}\langle r\rangle - \frac{C}{2}\left\langle\frac{1}{r}\right\rangle. \tag{43}$$

Adding the quark masses, this leads to

$$M = 2m_q + E = 2m_q + 2A\left\langle r^2\right\rangle + \frac{3B}{2}\langle r\rangle - \frac{C}{2}\left\langle\frac{1}{r}\right\rangle. \tag{44}$$

The mean square velocity is

$$\left\langle v^2\right\rangle = \frac{2}{M}\langle KE\rangle = \frac{2}{M}\left(A\left\langle r^2\right\rangle + \frac{B}{2}\langle r\rangle + \frac{C}{2}\left\langle\frac{1}{r}\right\rangle - D\left\langle\frac{1}{r^2}\right\rangle\right). \tag{45}$$

2.4 *Thermodynamic properties*

In this section, we provide numerical findings concerning the thermodynamic properties of selected meson systems. As demonstrated in Section 3, the KPIQP serves as a promising model for characterizing meson masses. The thermodynamic properties of the KPIQP can be derived from the partition function, which can be expressed as [50–52]:

$$Z(T) = \sum_{n=0}^{n_{\max}} e^{-\frac{E_{nl}}{k_B T}} = \sum_{n=0}^{n_{\max}} e^{-\beta E_{nl}} \tag{46}$$

where k_B is the Boltzmann constant, T is the absolute temperature, n is the principal quantum number ($n = 0,\ 1,\ 2,\ 3,\ldots$), and $n_{\max}$ is an upper bound of the vibrational quantum number, obtained from the numerical solution of $\frac{dE_{nl}}{dn} = 0$.

In the classical limit, at high temperature T, the sum can be replaced by an integral [23, 53], in which the partition function is defined as

$$Z(\beta) = \int_{n=0}^{n_{\max}} e^{-\beta E_{nl}} dn. \tag{47}$$

Integrating Eq. (40), we obtain the partition function as

$$Z(\beta) = \frac{1}{2}e^{-K\beta}\left[-Me^{-\frac{L\beta}{M^2}} + (M + 2n_{\max})e^{-\frac{L\beta}{(M+n_{\max})^2}} + \sqrt{L\pi\beta}\left(\mathrm{erfi}\left[\frac{\sqrt{L\beta}}{M}\right] - \mathrm{erfi}\left[\frac{\sqrt{L\beta}}{M + 2n_{\max}}\right]\right)\right] \tag{48}$$

where

$$M = \frac{3B}{\delta} + \frac{6A}{\delta^2} \tag{49}$$

$$L = 2\mu\left(\frac{3B}{\delta^2} + \frac{8A}{\delta^3} + C\right)^2 \tag{50}$$

$$K = 1 + \sqrt{\frac{8\mu B}{\hbar^2\delta^3} + ((N + 2l - 1)(N + 2l - 3) + 1) - \frac{8\mu D}{\hbar^2} + \frac{24\mu A}{\hbar^2\delta^4}} \tag{51}$$

$$n_{\max} = \frac{1}{2}\left(\sqrt{\frac{L}{K}} - M\right). \tag{52}$$

The imaginary error function $\mathrm{erfi}(x)$ is defined as follows:

$$\mathrm{erfi}(x) = \frac{2}{\sqrt{\pi}}\int_0^x e^{t^2} dt. \tag{53}$$

Table 1. Potential parameters obtained for each meson system. The units of A, B, D, and δ are GeV^3, GeV^2, GeV^{-1}, and GeV, respectively. C is dimensionless.

	Cornell potential	KPIQP
$c\bar{c}$	$A = D = 0$, $B = 0.224$, $C = 4.608$, $\delta = 0.216$	$A = 0.012$, $D = 2.458$, $B = 0.162$, $C = 4.997$, $\delta = 0.250$
$b\bar{b}$	$A = D = 0$, $B = 0.263$, $C = 2.570$, $\delta = 0.497$	$A = 0.0261$, $D = 0.100$, $B = 0.438$, $C = 2.034$, $\delta = 0.331$
$b\bar{c}$	$A = D = 0$, $B = 0.224$, $C = 7.340$, $\delta = 0.156$	$A = 0.012$, $D = 2.458$, $B = 0.162$, $C = 6.700$, $\delta = 0.180$
$c\bar{s}$	$A = D = 0$, $B = 0.306$, $C = 5.493$, $\delta = 0.449$	$A = 0.012$, $D = 2.458$, $B = 0.563$, $C = 7.656$, $\delta = 0.867$
$b\bar{s}$	$A = D = 0$, $B = 0.224$, $C = 5.315$, $\delta = 0.393$	$A = 0.012$, $D = 2.458$, $B = 0.162$, $C = 12.559$, $\delta = 0.305$
$b\bar{q}$	$A = D = 0$, $B = 0.224$, $C = 8.256$, $\delta = 0.256$	$A = 0.012$, $D = 2.458$, $B = 0.162$, $C = 7.640$, $\delta = 1.244$

3. Results and discussion

In the literature, the masses of the charm and bottom quarks are taken between 1.2 and 1.8 GeV and 4.8 and 5.3 GeV, respectively [54–56]. In this work, we have chosen $m_c = 1.209$ GeV, $m_b = 4.823$ GeV, $m_s = 0.419$ GeV, and $m_d = m_u = 0.220$ GeV [57, 58].

In this work, a Killingbeck potential combined with an inversely quadratic potential (KPIQP) is used to study some properties of mesons. The eigenvalues in the N-dimensional space and the corresponding wave functions are found by using the NU method.

The free parameters of the present calculations are A, B, C, D, and δ, which are fitted by fitting Eq. (40) in 3D space ($N = 3$) with the experimental data [59]. The results for the systems under consideration are given in Table 1. For each meson system, we substituted the experimental data into Eq. (40) and obtained the free parameters of the potential by solving the corresponding algebraic equations. For the charmonium and bottomonium mesons, we substituted the experimental values for the 1S, 2S, and 3S states into Eq. (40) to obtain the free parameters for the Cornell potential. However, for the KPIQP, we used data for the 1S, 2S, 3S, 1P, and 2P states to determine the free parameters. For the bottom–charm mesons, only two experimental values were available in the literature. We used the values of A, B, and D obtained from the charmonium fit with the 1S and 2S experimental data, which were then substituted into Eq. (40) to derive parameters C and δ. The free parameters for the charm–strange mesons were determined by inserting the parameter B and the experimental data for the 1S and 2S states into Eq. (40). This enabled us to determine the values of the parameters C and δ from two algebraic equations.

By using the potential parameters in Table 1, we plot in Fig. 1 the variations of the potential energy of the quark–antiquark interaction (Cornell potential and KPIQP) with the separation distance between the quark pairs, r, for the 1S state of different meson systems.

The plots obtained for the range of distances 0.1 fm $\leq r \leq$ 1 fm characteristic of charmonia and bottomonia have the same view as the plots of the potentials used in

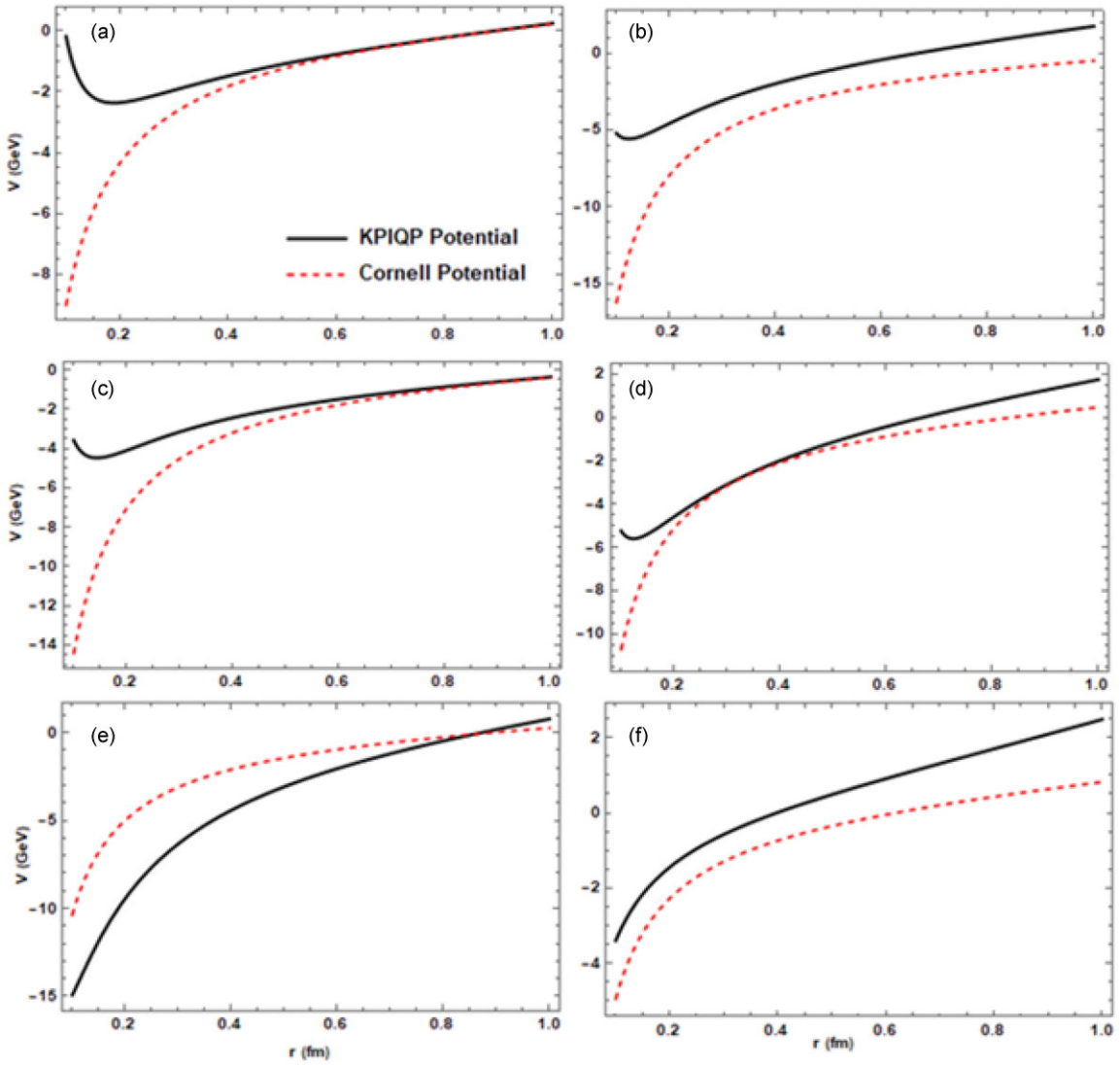

Fig. 1. The KPIQP (solid line) and the Cornell potential (dashed line) of the quark–antiquark interaction in (a) $c\bar{c}$, (b) $b\bar{b}$, (c) $b\bar{c}$, (d) $c\bar{s}$, (e) $b\bar{s}$, and (f) $b\bar{q}$ as a function of the quark–antiquark distance for the 1S state. The potential parameters are the same as in Table 1.

other works (see e.g. Refs. [60, 61]) for describing experimental data on these particle families.

By utilizing Eq. (40) and Table 1, we get the mass spectra of the different quantum states as shown in Tables 2–7. The obtained masses are in good agreement with experimental data, particularly for the S states. The slight deviations observed for the P states are attributed to the nonrelativistic approach used in our calculations. One needs to consider the spin–spin and spin–orbital interaction terms within the potential. Thus, the reason is not related to the correct choice of the parameters or making a better fit. These terms should be considered within the relativistic equations such as within the Klein–Fock–Gordon and Dirac equations.

We compared our findings with both experimental data [59] and results obtained using different methodologies, including the asymptotic iterative method (AIM) [26], the analytical ex-

Table 2. Charmonium ($c\bar{c}$) mass spectra energy in GeV.

States	Exp. [59]	Cornell	KPIQP	Ref. [26]	Ref. [27]	Ref. [28]	Ref. [29]	Ref. [30]	Relativistic [62]
1S	3.097	3.097	3.097	3.096	3.095 481	3.098	3.098	3.0963	3.096
2S	3.686	3.686	3.686	3.686	3.567 354	3.689	3.688	3.5681	3.686
3S	4.040	4.039	4.040	4.275	4.039 226	4.041	4.029	4.0400	4.088
4S	4.263	4.267	4.267	4.865	4.511 098	4.266		4.5119	
1P	3.525	3.297	3.396	3.214	3.567 735	3.262	3.516	3.5687	3.510
2P	3.773	3.802	3.902	3.773	4.039 607	3.784	3.925	4.0406	3.929
1D	3.770	3.585	3.784	3.412	4.039 683	3.515	3.779	4.0407	3.789
σ (%)		1.756	1.082	5.465	3.501	2.108	0.819	3.508	1.050

Table 3. Bottomonium ($b\bar{b}$) mass spectra energy in GeV.

States	Exp. [59]	Cornell	KPIQP	Ref. [26]	Ref. [27]	Ref. [28]	Ref. [29]	Ref. [30]	Relativistic [62]
1S	9.460	9.460	9.460	9.460	9.744 73	9.461	9.460	9.745	9.460
2S	10.023	10.023	10.023	10.023	10.023 15	10.023	10.026	10.023	10.023
3S	10.355	10.355	10.355	10.585	10.301 58	10.365	10.354	10.3016	10.355
4S	10.579	10.567	10.567	11.148	10.580 00	10.588	10.572	10.580	
1P	9.899	9.660	9.760	9.492	10.024 06	9.608	9.891	10.0246	9.892
2P	10.260	10.138	10.238	10.038	10.302 48	10.110	10.258	10.3029	10.255
1D	10.164	9.943	10.143	9.551	10.302 66	9.841	10.156	10.3032	10.153
σ (%)		0.842	0.277	2.844	0.940	1.110	0.041	0.942	0.038

Table 4. Bottom–charm ($b\bar{c}$) mass spectra energy in GeV.

States	Exp. [59]	Cornell	KPIQP	Ref. [26]	Ref. [27]	Ref. [28]	Ref. [29]	Ref. [30]	Relativistic [62]
1S	6.275	6.275	6.275	6.277	6.277 473	6.274	6.274	6.2770	6.332
2S	6.842	6.842	6.842	6.814	7.037 641	6.845	6.839	7.0372	6.881
3S		7.290	7.290	7.351	7.797 808	7.125	7.245	7.7973	7.235
4S		7.652	7.652	7.889	7.038 623	7.283	7.552		
1P		6.336	6.335	6.340	7.798 791	6.519	6.743	7.0381	6.734
2P		6.889	6.889	6.851		6.959	7.187	7.7983	7.126
1D		6.451	6.451	6.452		6.813	7.046		7.072

Table 5. Charm–strange ($c\bar{s}$) mass spectra energy in GeV.

States	Exp.	Cornell	KPIQP	Ref. [26]	Ref. [64]	Ref. [28]	Relativistic [65]
1S	1.968 49 [59]	1.968	1.968	2.512	1.968	1.969	2.129
2S	2.709 [63]	2.709	2.709	2.709	2.709	2.709	2.732
3S		3.054	3.054	2.906	2.932	2.913	3.193
4S		3.242	3.243	3.102		2.998	3.575
1P		2.452	2.550	2.649	2.566	2.601	2.549
2P		2.927	3.021	2.860		2.876	3.018
1D	2.859 [63]	2.859	2.859	2.859	2.857	2.862	2.899

Table 6. Bottom–strange ($b\bar{s}$) mass spectra energy in GeV.

States	Exp. [62, 66]	Cornell	KPIQP	Ref. [26]	Relativistic [65]
1S	5.415	5.415	5.415	5.415	5.450
2S		5.920	6.196	6.819	6.012
3S		6.128	6.594	8.225	6.429
4S		6.233	6.826	9.629	6.773
1P	5.830	5.830	5.830	5.830	5.857
2P		6.086	6.400	6.786	6.279
1D		6.072	6.268	6.264	6.182

Table 7. $\bar{q}$ mass spectra energy in GeV.

States	Exp. [62, 66]	Cornell	KPIQP	Ref. [26]	Relativistic [65]
1S	5.325	5.325	5.325	5.325	5.371
2S		5.765	6.331	6.413	5.933
3S		5.936	6.905	7.501	6.355
4S		6.017	6.262	8.589	6.703
1P	5.723	5.723	5.723	5.723	5.777
2P		5.916	6.550	6.786	6.197
1D		5.910	6.250	6.131	6.110

act iterative method (AEIM) [27], the Wentzel–Kramers–Brillouin method (WKB) [28], the Laplace transformation method (LTM) [29], the artificial neural network method (ANN) [30], and a relativistic model [62]. Additionally, we calculated the average deviations between our results and those obtained through different methods from available experimental data. The average deviation is defined as:

$$\sigma\ (\%) = \frac{100}{N} \sum \left| \frac{M_{nl}\,(\mathrm{Exp}) - M_{nl}\,(\mathrm{cal})}{M_{nl}\,(\mathrm{Exp})} \right|$$

where N is the number of experimental data points, and $M_{nl}(\mathrm{Exp})$ and $M_{nl}(\mathrm{cal})$ are the experimental mass and the calculated mass, respectively. We found that the KPIQP is better than the Cornell potential in modeling the mass spectra of meson systems.

It is worth noting that, despite the Cornell potential having fewer parameters compared to the KPIQP, the resulting outcomes are not significantly different. Therefore, we may conclude that our observation for the meson masses does not depend much more on the number of parameters. Besides that, our results are improved in comparison with the results obtained by other methods, as shown in Tables 2–7.

We investigated the variations of the mass spectra energy of the systems under consideration as a function of the parameter δ for different states. The results are shown in Fig. 2. We observed a consistent decrease as the potential strength δ increases. Figure 3 displays the variations of charmonium ($c\bar{c}$) and bottomonium ($b\bar{b}$) mass spectra energy as a function of the

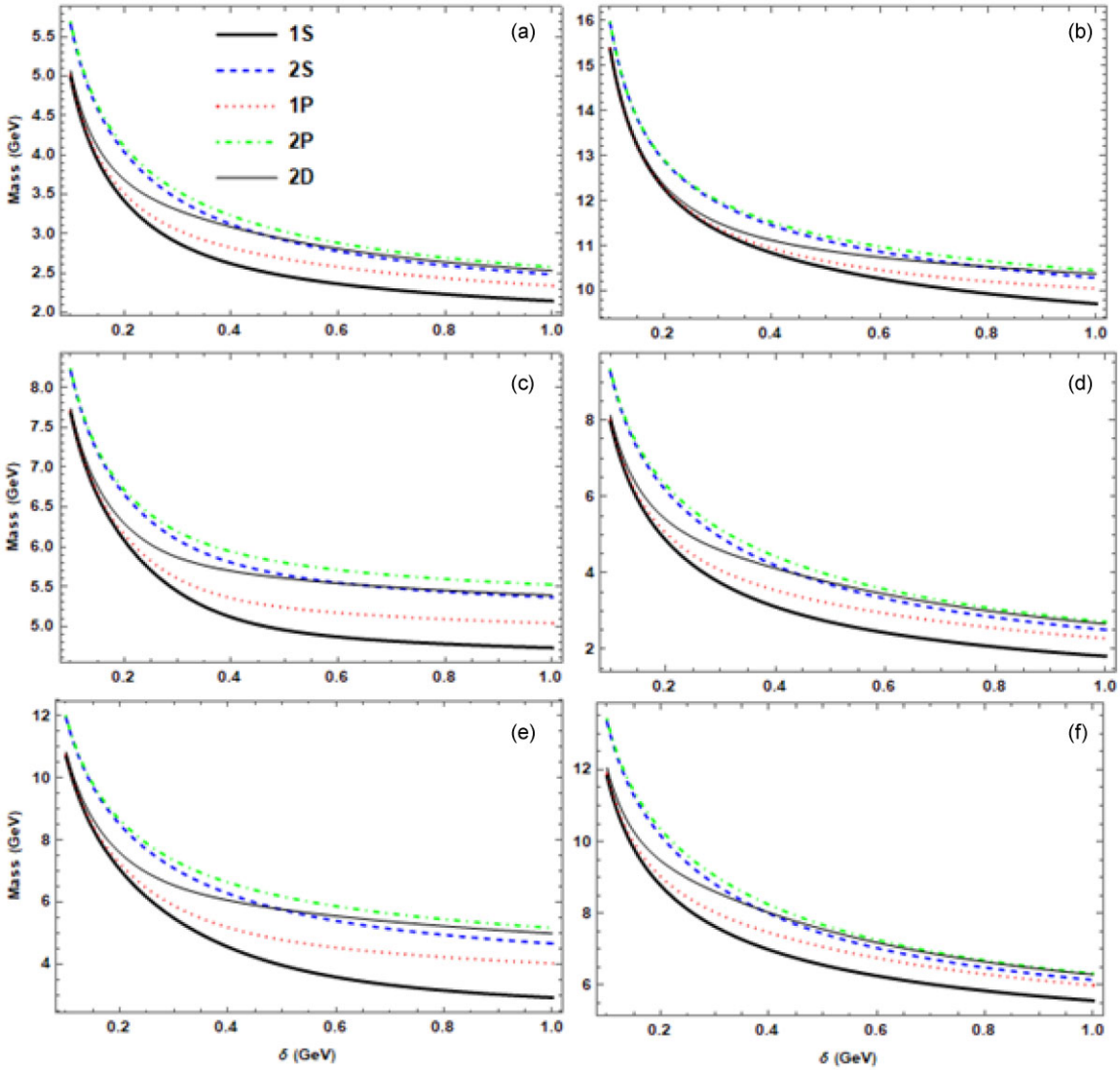

Fig. 2. Variation of the mass spectra energy with the parameter δ of (a) $c\bar{c}$, (b) $b\bar{b}$, (c) $b\bar{c}$, (d) $c\bar{s}$, (e) $b\bar{s}$, and (f) $b\bar{q}$ for the 1S, 2S, 1P, and 2D states. The potential parameters are the same as in Table 1.

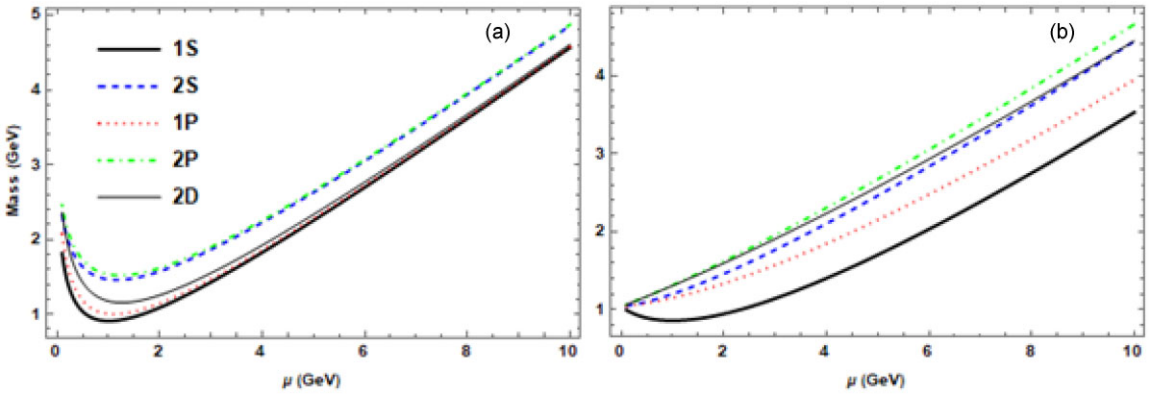

Fig. 3. Variation of the mass spectra energy with the reduced mass of charmonium and bottomonium for the 1S, 2S, 1P, and 2D states. The potential parameters are the same as in Table 1.

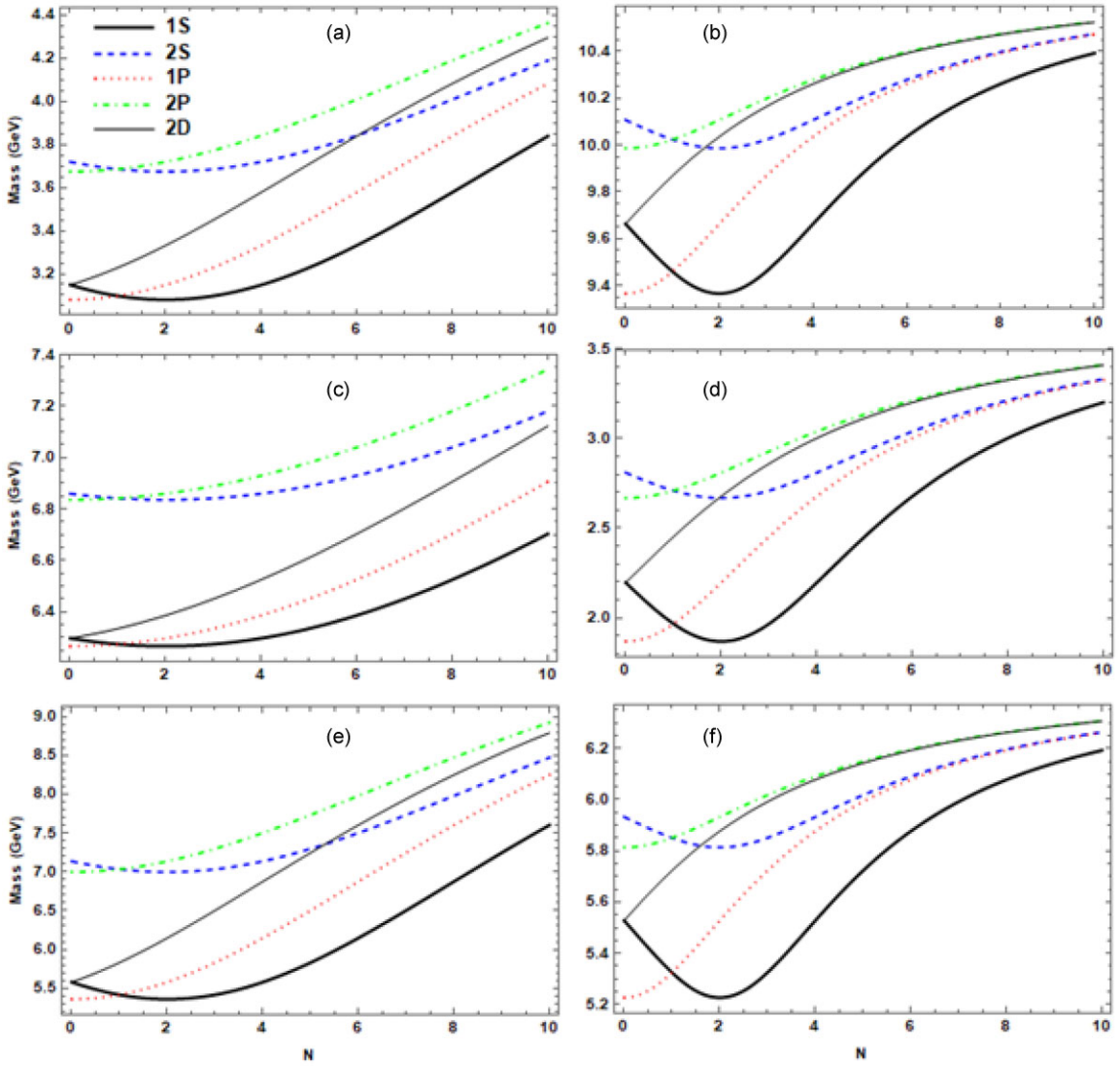

Fig. 4. Variation of the mass spectra energy with the dimensional number N of (a) $c\bar{c}$, (b) $b\bar{b}$, (c) $b\bar{c}$, (d) $c\bar{s}$, (e) $b\bar{s}$, and (f) $b\bar{q}$ for the 1S, 2S, 1P, and 2D states. The potential parameters are the same as in Table 1.

reduced mass μ for different states. The mass spectra energy initially decreases to a minimum and then increases as the reduced mass μ increases, with this behavior observed across various angular quantum numbers.

We also investigated the effect of the dimensional number on the masses of mesons. The results are graphically presented in Fig. 4. We observed that the charmonium mass increases with increasing dimensional number for P and D states due to the increasing binding energy. Therefore, the binding energy is larger than the constituents of charmonium, giving us the limitations of nonrelativistic models. The effect of dimensionality is the same as that of charmonium for all other studied meson systems. However, it is easily seen that the S state seems to be unlike the other states. The mass decreases when the dimensional number is less than 3 and then increases for higher dimensional numbers.

Table 8. Radii of charmonium and bottomonium in fm.

States	Present work	Ref. [67]	Ref. [68]	Present work	Ref. [67]	Ref. [68]
1S	0.397	0.439	0.41	0.186	0.225	0.233
2S	0.852	0.915	0.91	0.448	0.488	0.545
3S	1.237	1.352	1.38	0.657	0.737	0.805
4S	1.740	1.762	1.87	0.937	0.972	1.030
1P	0.676	0.697	0.71	0.364	0.370	0.435
2P	1.091	1.155	1.19	0.583	0.628	0.711
1D	0.896	0.936	0.96	0.502	0.507	0.593

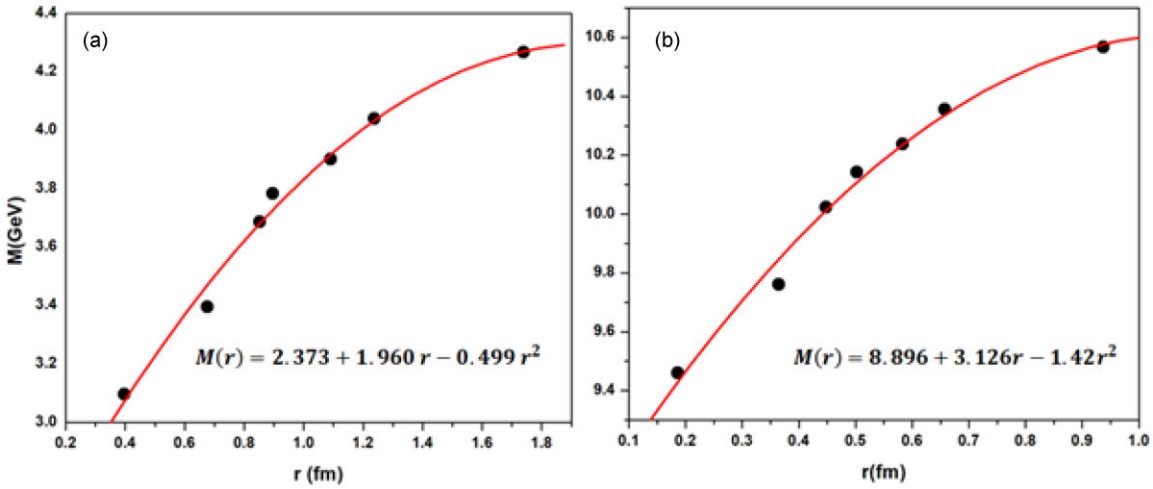

Fig. 5. Variation of the mass as a function of the radius of the states of charmonium (a) and bottomonium (b). The solid line corresponds to a quadratic fit.

Using the parameters in Table 1 and Eq. (41), we computed the radii ($r_{\rm rms}$) for different states of charmonium and bottomonium. The obtained results are listed in Table 8 and are in good agreement with the values obtained for other potential energy functions in the existing literature [67, 68]. The results show the validity of the method used. From Table 8, we observe that bottomonium objects are more compact than the corresponding charmonium ones. Furthermore, the charmonium sizes are roughly twice as large as those of similar states of bottomonium.

Finally, we investigated the mass–radius dependence for charmonium and bottomonium including all states. Figure 5 shows the variation of the charmonium and bottomonium masses obtained by our calculation (from Tables 2 and 3) as a function of the radii provided in Table 8. A quadratic fit reflects perfectly the dependence of mass and radius (solid line in Fig. 5). The equations corresponding to the fitted curve are provided alongside the figure. We find that all the states that we considered are dominated by the quadratic part of the potential and thus

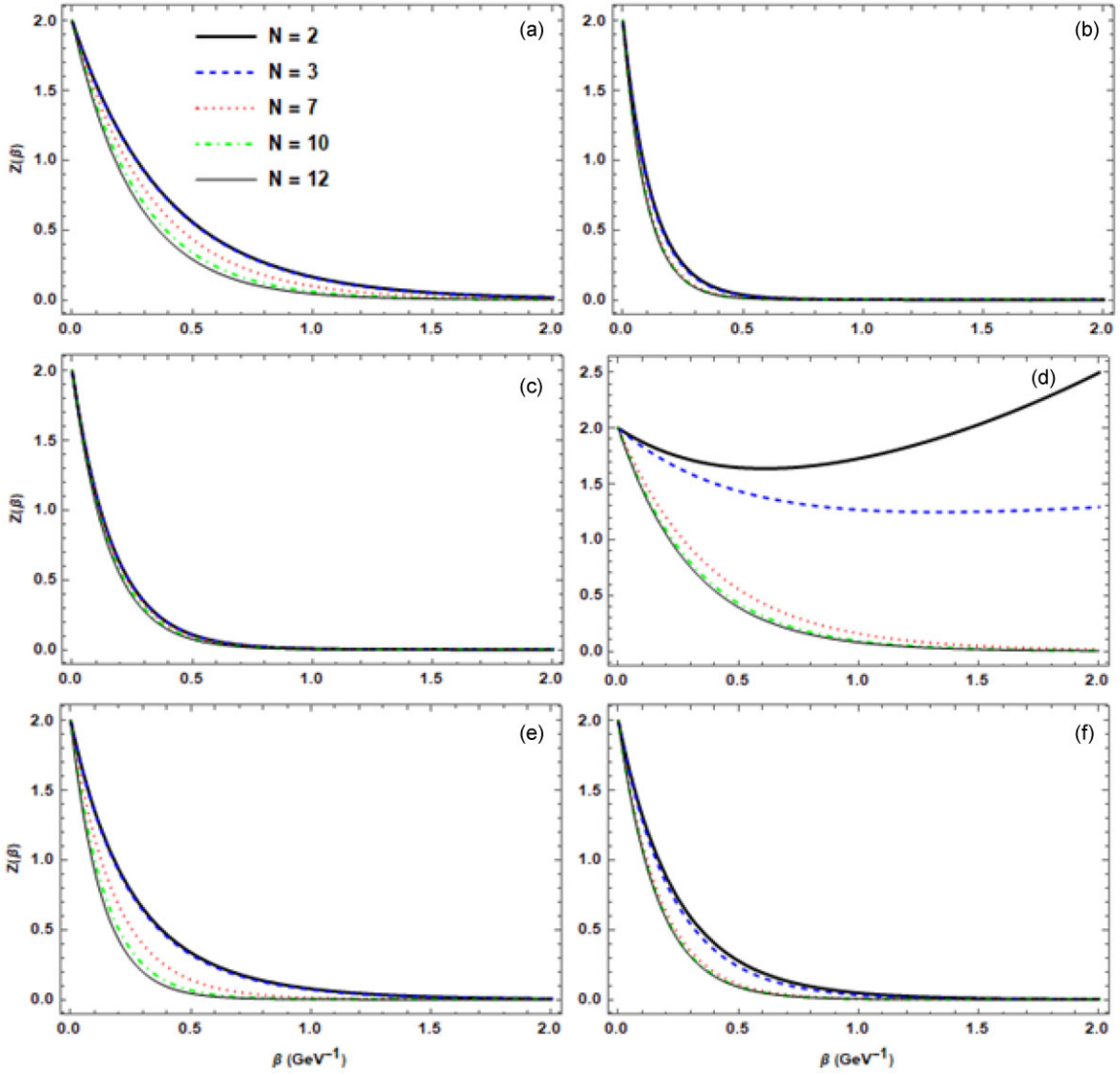

Fig. 6. Variation of the partition function as a function of $\boldsymbol{\beta}$ for different dimensional numbers: (a) $\boldsymbol{c\bar{c}}$, (b) $\boldsymbol{b\bar{b}}$, (c) $\boldsymbol{b\bar{c}}$, (d) $\boldsymbol{c\bar{s}}$, (e) $\boldsymbol{b\bar{s}}$, and (f) $\boldsymbol{b\bar{q}}$. The potential parameters are the same as in Table 1.

the small correction from the Coulomb term in the quadratic mass–radius relation (50) can be neglected.

The thermal properties for the studied meson systems (for the 1S state) are plotted as shown in Figs. 6–10. Figure 6 shows that the partition function of mesons (1S state) decreases as the parameter β increases (the temperature decreases). Notably, at certain temperature values, the partition function remains constant. The observed results are in agreement with the findings reported in Refs. [25, 66, 67]. We note that, at a certain temperature range, the meson melts to its constituent quarks. Additionally, increasing the dimensional number leads to an overall decrease in the partition function across all meson systems under consideration.

In Fig. 7, we see that the mean energy of mesons consistently decreases as β increases, which is in agreement with other works [25, 69, 70]. However, the mean energy increases with increasing dimensional number. This effect was likewise observed in Ref. [25].

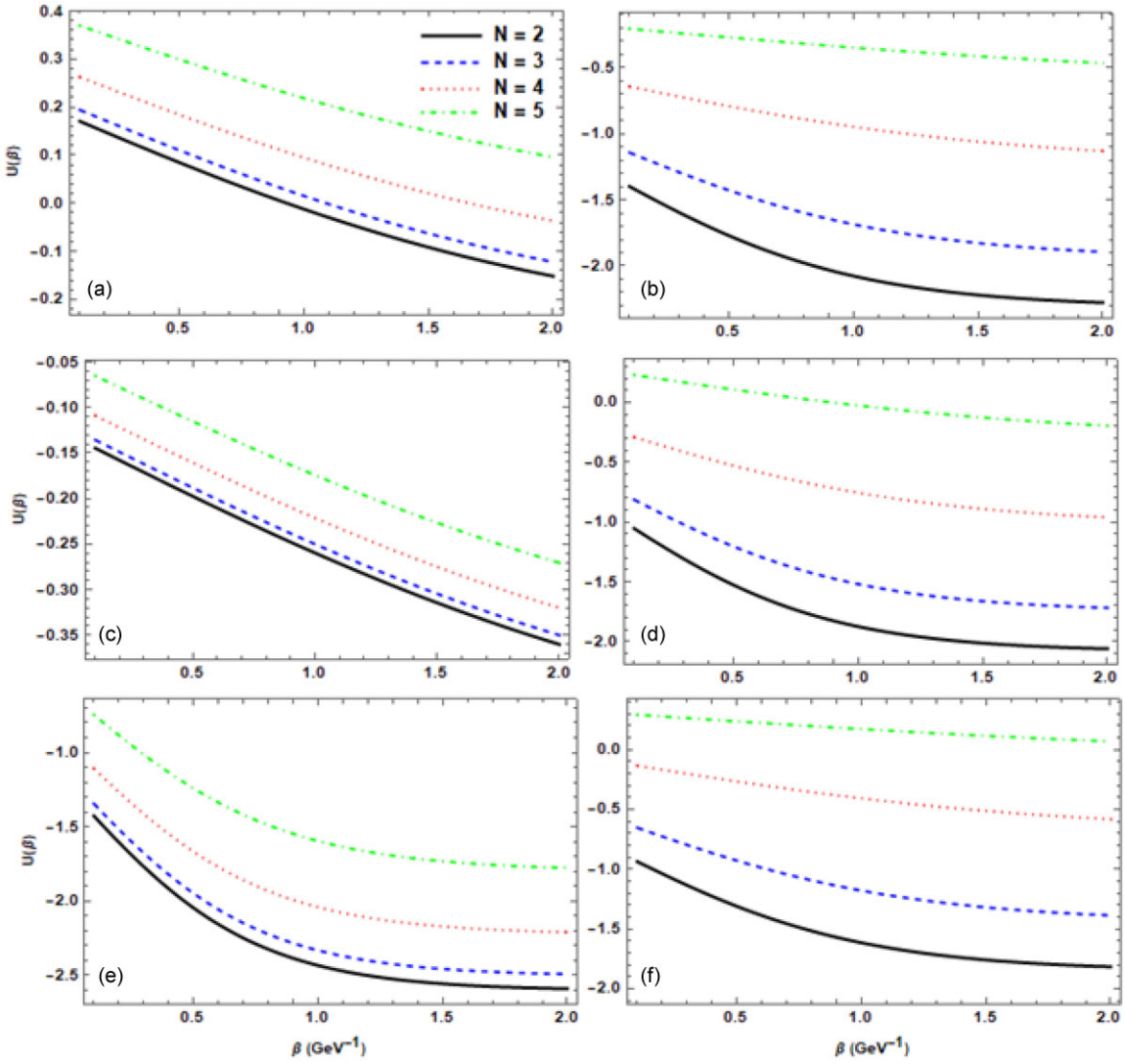

Fig. 7. Variation of the mean energy as a function of $\boldsymbol{\beta}$ for different dimensional numbers: (a) $\boldsymbol{c\bar{c}}$, (b) $\boldsymbol{b\bar{b}}$, (c) $\boldsymbol{b\bar{c}}$, (d) $\boldsymbol{c\bar{s}}$, (e) $\boldsymbol{b\bar{s}}$, and (f) $\boldsymbol{b\bar{q}}$. The potential parameters are the same as in Table 1.

Figure 8 shows that the free energy increases as β increases (the temperature decreases). As β approaches a certain value, the free energy tends to stabilize. This behavior of charm quark matter is in qualitative agreement with the findings of Refs. [37, 71]. Furthermore, the free energy increases with increasing dimensional number.

The variation of specific heat capacity with β for various dimensional numbers is displayed in Fig. 9. The specific heat capacity increases to a peak and then decreases towards zero as β increases. In addition, Fig. 9 indicates that the peak position of the specific heat capacity shifts to higher β values with increasing dimensionality. The specific heat behavior has been previously studied and our findings are in qualitative agreement with the studies in Refs. [69, 70].

The variation of the entropy as a function of β for various dimensional numbers is plotted in Fig. 10. We observe that the entropy decreases as β increases. In addition, the entropy shifts

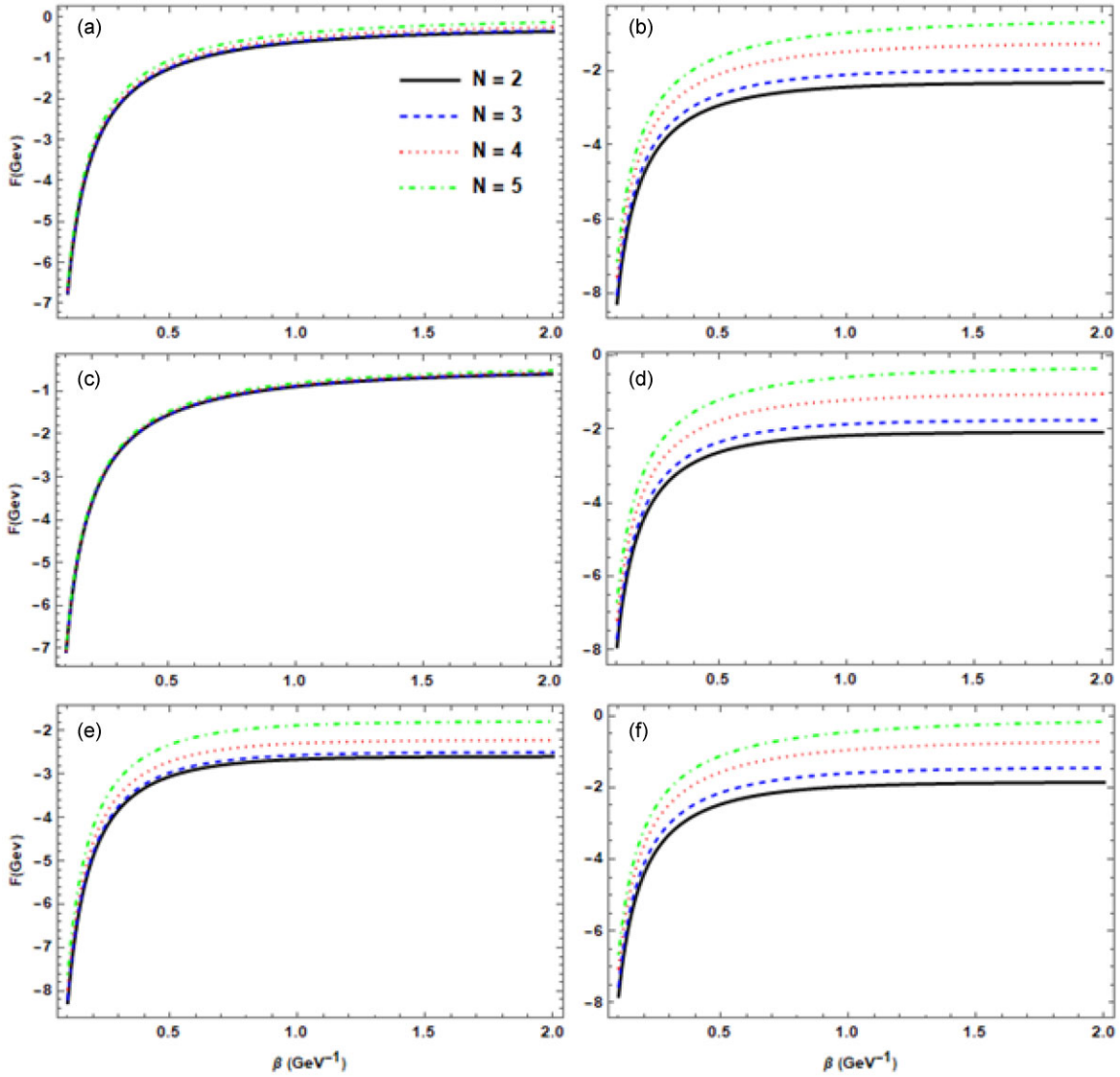

Fig. 8. Variation of the free energy as a function of $\boldsymbol{\beta}$ for different dimensional numbers: (a) $\boldsymbol{c\bar{c}}$, (b) $\boldsymbol{b\bar{b}}$, (c) $\boldsymbol{b\bar{c}}$, (d) $\boldsymbol{c\bar{s}}$, (e) $\boldsymbol{b\bar{s}}$, and (f) $\boldsymbol{b\bar{q}}$. The potential parameters are the same as in Table 1.

to higher values with increasing dimensional number N. We obtained the same conclusion as in Ref. [70].

4. Conclusions

In the present study, we employ the Nikiforov–Uvarov method (NU) for determining the energy eigenvalues and the wave functions of the multidimensional radial Schrödinger equation with the Killingbeck potential combined with an inversely quadratic potential (KPIQP).

The meson masses are analytically obtained in the N-dimensional space and special cases are obtained in comparison with other studies. The effect of the dimensional number on the mass spectra of different mesons is studied. The results show excellent agreement in comparison with experimental data and the results obtained by alternative analytical methods, which offers new insights into the properties of interactions in hadronic systems.

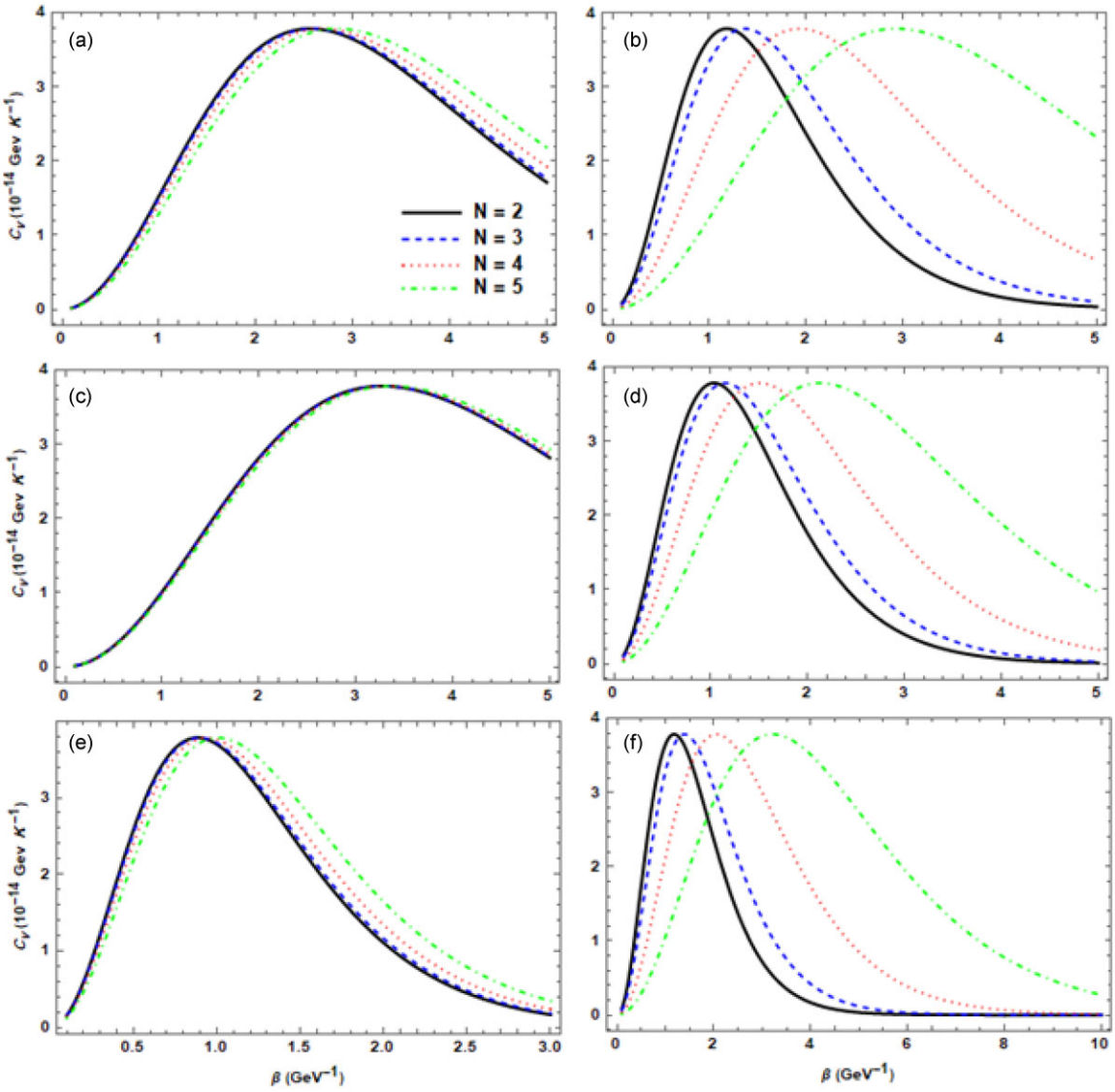

Fig. 9. Variation of the specific heat capacity as a function of $\boldsymbol{\beta}$ for different dimensional numbers: (a) $\boldsymbol{c\bar{c}}$, (b) $\boldsymbol{b\bar{b}}$, (c) $\boldsymbol{b\bar{c}}$, (d) $\boldsymbol{c\bar{s}}$, (e) $\boldsymbol{b\bar{s}}$, and (f) $\boldsymbol{b\bar{q}}$. The potential parameters are the same as in Table 1.

In addition, the mean radii of the bound states of the charmonium meson and the bottomonium meson are computed. The radius of $b\bar{b}$ is smaller than the radius of $c\bar{c}$. This observation refers to one of the characteristics of quarkonium that heavy quarkonia have smaller radii.

The relationships between the theoretical masses that we obtained and the radii are shown. As pointed out previously, the quadratic fit reflects perfectly the dependence of mass and radius.

Finally, our investigation explored the thermodynamic properties of mesons, including free energy, internal energy, entropy, and specific heat capacity, across different selected dimensionalities. Through various plots, we have identified distinct behaviors of these thermodynamic properties as they vary with temperature. The effect of the dimensional number on the thermodynamic properties of mesons is investigated. We noted from the figures that the internal energy, the free energy, the specific heat, and the entropy shift to higher values with increasing

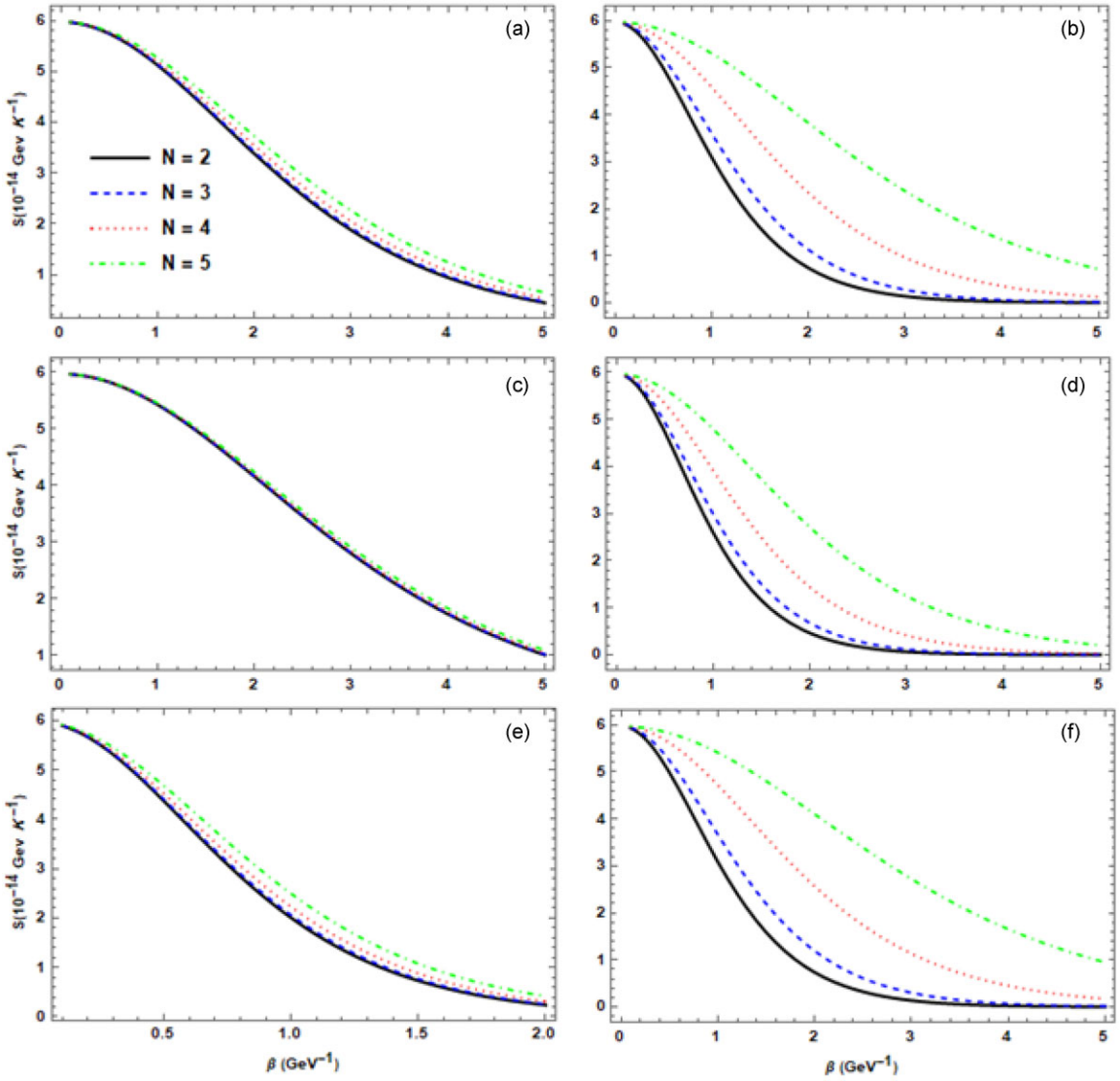

Fig. 10. Variation of the entropy as a function of β for different dimensional numbers: (a) $c\bar{c}$, (b) $b\bar{b}$, (c) $b\bar{c}$, (d) $c\bar{s}$, (e) $b\bar{s}$, and (f) $b\bar{q}$. The potential parameters are the same as in Table 1.

dimensional number. This work will be extended to include spin–spin interaction and spin–orbital interaction. In addition, the effect of external magnetic field on heavy meson properties, which gives more information about the quark–gluon plasma, will be studied in future work.

Acknowledgment

The authors would like to thank the anonymous reviewers for their time and valuable feedback, which has greatly contributed to improving the quality of this manuscript.

Data availability statement

The authors declare that the data supporting the findings of this study are available on request from the corresponding author (R. H).

Appendix. Overview of the Nikiforov–Uvarov method

The Nikiforov–Uvarov (NU) method is based on the solutions to a generalized second-order linear differential equation with special orthogonal functions [18]. A Schrödinger equation of the type

$$\psi_n^{''}(\mathrm{s}) + (E - V(s))\,\psi_n(s) = 0 \tag{A1}$$

could be solved by this method. This can be done by transforming Eq. (A1) into an equation of hypergeometric type with appropriate coordinate transformation $z = z(r)$ to get

$$\psi_n^{''}(\mathrm{s}) + \frac{\tilde{\tau}(\mathrm{s})}{\sigma(\mathrm{s})}\psi'(\mathrm{s}) + \frac{\tilde{\sigma}(\mathrm{s})}{\sigma^2(\mathrm{s})}\psi_n(s) = 0, \tag{A2}$$

where $\sigma(\mathrm{s})$ and $\tilde{\sigma}(\mathrm{s})$ are polynomials, at most of second degree, and $\tilde{\tau}(\mathrm{s})$ is a first-degree polynomial.

In order to find the exact solution to Eq. (A1), we set the wave function as

$$\psi_n(s) = \phi_n(s)\,\mathrm{y}_n(s). \tag{A3}$$

Substituting Eq. (A3) into Eq. (A2) reduces Eq. (A2) into a hypergeometric type, given as

$$\sigma(s)\,\phi_n^{''}(s) + \tau(s)\,y_n'(s) + \lambda \mathrm{y}_n(s) = 0 \tag{A4}$$

where the wave function $\phi_n(s)$ is defined as the logarithmic derivative:

$$\frac{\phi_n'(s)}{\phi_n(s)} = \frac{\pi(s)}{\sigma(s)} \tag{A5}$$

where $\pi(s)$ is at most a first-degree polynomial. In addition, the hypergeometric type function $\mathrm{y}_n(s)$ in Eq. (4) for a fixed n is given by the Rodrigues relation:

$$\mathrm{y}_n(s) = \frac{B_n}{\rho(s)}\frac{d^n}{ds^n}\left[\sigma^n(s)\,\rho(s)\right] \tag{A6}$$

where B_n is the normalization constant and the weight function, $\rho(s)$ must satisfy the condition:

$$(\sigma(s)\,\rho(s))' = \tau(s)\,\rho(s) \tag{A7}$$

with

$$\tau(s) = \tilde{\tau}(s) + 2\pi(s). \tag{A8}$$

For the weight function $\rho(s)$ to be satisfied, it is necessary that the classical orthogonal polynomials $\tau(s)$ be equal to zero in an interval (a, b) and its derivative at this interval at $\sigma(s) > 0$ be negative. That is,

$$\tau'(s) = 0. \tag{A9}$$

Thus, the function $\pi(s)$ and the parameter λ required for the NU methods are defined as follows
:

$$\pi(s) = \frac{\sigma' - \tilde{\tau}}{2} \pm \sqrt{\left(\frac{\sigma' - \tilde{\tau}}{2}\right)^2 - \tilde{\sigma} + k\sigma} \tag{A10}$$

$$\lambda = k + \pi'(s). \tag{A11}$$

The k-values in the square root of Eq. (A11) can be evaluated if the expression under the square root is the square of the polynomials. This is possible if and only if its discriminant is zero. Therefore, the new eigenvalue equation for the Schrödinger equation becomes

$$\lambda = \lambda_n = -n\tau' - \frac{n(n-1)\,\sigma''}{2},\ n = 0,\ 1,\ 2\ldots \tag{A12}$$

On comparing Eqs. (A11) and (A12), we obtain the energy eigenvalues.

Furthermore, the other part $y_n(s)$ of the wave function in Eq. (33) is a hypergeometric-type function whose polynomial solutions are given by the Rodrigues relation:

$$y_n(s) = \frac{B_n}{\rho(s)} \frac{d^n}{ds^n} \left(\sigma^n(s)\,\rho(s)\right) \tag{A13}$$

where B_n is a normalizing constant and the weight function $\rho(s)$ must satisfy the condition [18]

$$(\sigma\,\rho)' = \tau\,\rho. \tag{A14}$$

References

[1] K. A. Olive, Chin. Phys. C **38**, 090001 (2014).
[2] A. Ali, (2011) arXiv preprint, arXiv:1108.2197.
[3] M. Gersabeck, Mod. Phys. Lett. A **27**, 1230026 (2012).
[4] S. L. Olsen, Prog. Theor. Phys. Suppl. **193**, 38 (2012).
[5] L. Li, Nucl. Phys. B Proc. Suppl. **225–227**, 107 (2012).
[6] N. Brambilla, et al. Eur. Phys. J. C **71**, 1–178 (2011).
[7] N. Brambilla, et al., Eur. Phys. J. C **74** 2981 (2014)
[8] Y.-L. Ma, arXiv preprint, arXiv:0906.3842 (2009).
[9] R. L. Jaffe, Phys. Rev. Lett. **38**, 195 (1977); **38**, 617 (1977) [erratum].
[10] R. J. Jaffe, Phys. Rev. D **15**, 267 (1977).
[11] J. Weinstein and N. Isgur, Phys. Rev. D **27**, 588 (1983).
[12] J. Weinstein and N. Isgur, Phys. Rev. D **41**, 2236 (1990).
[13] J. Weinstein, Phys. Rev. D **47**, 911 (1993).
[14] A. I. Ahmadov, C. Aydin, and O. Uzun, J. Phys.: Conf. Ser. **1194**, 012001 (2019).
[15] M. Abu-Shady, T. A. Abdel-Karim, and E. M. Khokha, Adv. High Energy Phys. **2018**, 7356843 (2018).
[16] M. Abu-Shady, Egypt. Math. Soc. **25**, 86 (2017).
[17] S. M. Kuchin and N.V. Maksimenko, Universal J. Phys. Appl. **7**, 295 (2013).
[18] A. Al-Jamel and H. Widyan, Appl. Phys. Res. **4**, 94 (2012).
[19] G. Bhanot and S. Rudaz, Phys. Lett. B. **78**, 119 (1978).
[20] S. M. Kuchin and N. V. Maksimenko, Universal J. Phys. Appl. **7**, 295 (2013).
[21] R. Horchani, N. Al-Kindi, and H. Jelassi, Mol. Phys. **119**(4), e1812746 (2020).
[22] A. I. Ahmadov, C. Aydin, and O. Uzun, Phys. Conf. Ser. **1194**, 012001 (2019).
[23] I. B. Okon et al., Sci Rep. **13**, 8193 (2023).
[24] H. Mansour and A. Gamal, Adv. High Energy Phys. **2018**, 7269657 (2018).
[25] M. Abu-Shady, T. A. Abdel-Karim, and Y. Sh., Egypt. Math. Soc. **27**, 14(2019).
[26] R. Rani, S. B. Bhardwaj, and F. Chand, Commun. Theor. Phys. **70**, 179 (2018).
[27] E. M. Khokha, M. Abu-Shady, and T. A. Abdel-Karim, Int. Theor. Appl. Math. **2**, 86 (2016).
[28] E. Omugbe, O. E. Osafile, and M. C. Onyeaju, Adv. High Energy Phys. **2020**, 5901464 (2020).
[29] M. Abu-Shady, T. A. Abdel-Karim, and E. M. Khokha, SciFed J. Quantum Phys. **2**, 1–11(2018).
[30] H. Mutuk, Adv. High Energy Phys. **2019**, 3105373 (2019).
[31] Y. Nemoto, K. Naito, and M. Oka, Eur. Phys. J. A **9**, 245 (2000).
[32] M. Abu-Shady, Int. J. Theor. Phys. **49**, 2425 (2010).
[33] M. Abu-Shady and M. Soleiman, Phys. Part. Nucl. Lett. **10**, 683 (2013).
[34] M. Abu-Shady, T. A. Abdel-Karim, and E. M. Khokha, Adv. High Energy Phys. **2018**, 7356843 (2018).
[35] S. Roy and D. K. Choudhury, Can. Phys. **94**, 1282 (2016).
[36] J. Kretzschmar, Nucl. Part. Phys. Proc. **273–275**, 541 (2016).
[37] M. Modarres and A. Mohamadnejad, Phys. Part. Nucl. Lett. **10**, 99 (2013).
[38] M. Abu-Shady, Int. Theor. Phys. **54**, 1530 (2015).
[39] N. V. Maksimenko and S. M. Kuchin, Phys. Part. Nucl. Lett. **9**, 134 (2012).
[40] S. M Ikhdair, Adv. High Energy Phys. **2013**, 491648 (2013).
[41] H. Mutuk, Adv. High Energy Phys. **2019**, 3105373 (2019).
[42] R. Rani and F. Chand, Indian Phys. **92**, 145 (2018).
[43] R. Rani and F. Chand, Appl. Sci. Lett. **2**, 129 (2016).

[44] R. Rani, S. B. Bhardwaj, and F. Chand, Pramana **91**, 1 (2018).
[45] H. Hassanabadi, B. H. Yazarloo, S. Zarrinkamar, and M. Solaimani, Int. J. Quantum Chem. **112**, 3706 (2012).
[46] E. Omugbe, O. E. Osafile, and M. C. Onyeaju, Adv. High Energy Phys. **2020**, 5901464 (2020).
[47] A. K. Rai, B. Patel, and P. C. Vinodkumar, Phys. Rev. C **78**, 055202 (2008).
[48] A. K. Rai, J. N. Pandya, and P. C. Vinodkumar, J. Phys. G: Nucl. Part. Phys. **31**, 1453 (2005).
[49] P. Gupta and I. Mehrotra, Mod. Phys. **3**, 1530 (2012).
[50] W. A. Yah and K. J. Oyew, J. Assoc. Arab Univ. Basic Appl. Sci. **21**, 53 (2016).
[51] R. Horchani and H. Jelassi, South African J. Chem. Eng. **33**, 103 (2020).
[52] R. Horchani and H. Jelassi, Chem. Phys. Lett. **753**, 137583 (2020).
[53] R. Horchani, H. Al-Aamri, N. Al-Kindi, A. N. Ikot, U. S. Okorie, G. J. Rampho, and H. Jelassi, Eur. Phys. D **75**, 1–13 (2021).
[54] B. Patel and P. C. Vinodkumar, J. Phys. G: Nucl. Part. Phys. **36**, 035003 (2009).
[55] A. A. Rajabi, J. Sci. **16**, 73 (2005).
[56] N. V. Maksimenko and S. M. Kuchin, Russ. Phys. **54**, 57 (2011).
[57] S. Godfrey, K. Moats, and E. S. Swanson, Phys. Rev. D **94**, 054025 (2016).
[58] S. Godfrey and K. Moats, Phys. Rev. D **92**, 054034 (2015).
[59] C. Patrignani, Chin. Phys. C **40**, 100001 (2016).
[60] A. A. Bykov, I. M. Dremin, and A. V. Leonidov, Usp. Fiz. Nauk **143**, 3 (1984).
[61] H. Ciftci, R. L. Hall, and Q. D. Katatbeh, J. Phys. A: Math. Gen. **36**, 7001 (2003).
[62] D. Ebert, R. N. Faustov, and V. O. Galkin, Phys. Rev. D **67**, 014027 (2003).
[63] K. A. Olive, Chin. Phys. C **38**, 090001 (2014).
[64] M. Abu-Shady, arXiv preprint, arXiv:1504.07538 (2015).
[65] S. Godfrey and K. Moats, Phys. Rev. D **93**, 034035 (2016).
[66] J. Beringer et al. Phys. Rev. D **86**, 1, 1504 (2012).
[67] R. Manzoor, J. Ahmed, and A. Raya, Rev. Mex. Fis. **67**, 33 (2021).
[68] J. T. Laverty, S. F. Radford, and W. W. Repko, (2009). arXiv preprint, arXiv:0901.3917.
[69] A. N. Ikot, U. S. Okorie, P. Sawangtong, M. E. Udoh, S. Zare, and H. Hassanabadi, Eur. Phys. Plus **131**, 1 (2016).
[70] H. Hassanabadi and M. Hosseinpour, Eur. Phys. C **76**, 1 (2016).
[71] M. Modarres and H. Gholizade, Int. Mod. Phys. E **17**, 1335 (2008).